Ionic liquids, possessing inherent polar character, are mainly considered as green solvents due to extremely low vapour pressure and almost non-volatile behavior [Bhushan et al. (2010)]. Because of high thermal and chemical stability, ionic liquids themselves may be used as synthetic lubricants. Since these are expensive chemicals, it is better to use them as an additive to a base lubricant rather than as lubricant itself [Qu et al. (2017), Liu et al. (2009)]. Some reports are available in literature where ionic liquids have been used for functionalization of graphene [Kumar et al. (2019) Wang et al. (2018)], stabilization of nanoparticles [Kheireddin et al. (2013)] /quantum dots [Liu et al. (2017) Mou et al. (2019), Wang et al. (2016)] / carbon nanotubes [Yu et al. (2015)]. Properties of ionic liquids may be regulated by selection of appropriate cation or anion in ionic liquid. Several ionic liquids, cation based like imidazolium [Zhang et al. (2012) Jimenez et al. (2006) (2008a)], ammonium [Gusain et al. (2014) Fu et al. (2015), Li et al. (2017)], pyridinium [Mahrova et al. (2015)], phosphonium [Westerholt et al. (2015), Valbe et al. (2017)] etc., anion based such as tetrafluoro borate $[BF_4]^-$, hexafluoro phosphate $[PF_6]^-$, [Sulfonate], (trifluoromethylsulfonyl) imide $[Tf_2N]^-$, (2-ethylhexyl) phosphate [DEHP] etc. and mixed ionic liquid have been used in the field of tribology [Qu et al. (2017)].

A variety of inorganic nanoparticles of metals, metal oxides, metal sulfides, metal fluorides and carbon-based materials have been applied to reduce friction and wear [Verma et al. (2019)]. It has also been established that doping of nanoparticles with some other ion Mg, Cu, N in ZnO [Kalyani et al. (2016), Zhang et al. (2013)], La, Ce in TiO_2 [Gu et al. (2013) (2013a)], Cu, Re in MoS_2 [Li et al. (2019), Yadgarov et al. (2013)], Ca, Al, Y in ZrO_2 [Relyski et al. (2020)] has improved the tribological properties. Oleic acid capped lead sulfide nanoparticles have provided very high

activity [Liu et al. (2006)]. Qu and his team have studied organic-modified silver nanoparticles as lubricant additives [Qu et al. (2017)]. Tribological properties of sodium dodecyl sulfate (SDS) stabilized magnesium doped zinc oxide nanoparticles [Kalyani et al. (2016)], and stearic acid stabilized calcium copper titanate nanoparticles [Rastogi et al. (2014)] have been reported from our laboratory. Antiwear performance of phosphonium based ionic liquids mixed with stabilized oxide nanoparticles in PAO and 5w40 has been reported [Valbe et al. (2017)].

Given the above, it appeared us intriguing to synthesize calcium doped ceria nanoparticles (CCO), modify their surface with sodium dodecyl sulfate, 1-decyl-3-methyl imidazolium bis (trifluoromethylsulfonyl) imide and compare their tribological efficiency in paraffin oil (PO).

4.1. Experimental Section

4.1.1. Chemicals

The chemicals ceric ammonium nitrate, calcium nitrate,1-decyl 3-methyl imidazolium bis (trifluoromethylsulfonyl) imide, citric acid and dimethyl formamide (DMF) used in this work were of AR grade and used without further purification.

4.1.2. Synthesis of lubricant additives

4.1.2.1. Synthesis of Ca doped Ceria nanoparticles

The Ca-doped ceria (CCO) NPs have been synthesized by sol-gel method. 50 mL aqueous solution containing ceric ammonium nitrate (6.35 g), calcium nitrate (0.151 g) and citric acid (1.487 g) was stirred continuously at 200 ± 5 °C until it formed gel and

ultimately burnt. The obtained blackish ash was calcined at 400 °C in air for 2 h [Ramasamy et al. (2018)].

4.1.2.2. Synthesis of IL modified Ca doped Ceria nanoparticles

Ionic liquid [(1-decyl 3-methyl imidazolium bis (trifluoromethylsulfonyl) imide] and CCO, both 0.5 gm each in 20mL DMF, were ultrasonicated separately for 1h. The solutions were mixed and stirred overnight at room temperature. The solvent DMF was evaporated. The residual DMF was removed by adding methanol, and the product was dried *in vacuo.*

4.1.3. Sample Preparation

The blends of additives with PO were made in varying concentrations 0.1, 0.2, 0.3 and 0.4 % (w/v) using a magnetic stirrer at 40-50 °C for 2h and then sonicated for 1h. The antiwear and load-carrying tests were carried out at an optimized concentration, i.e., 0.2% w/v of CCO, SCCO, IL-CCO in paraffin oil.

4.2. Results and discussion

4.2.1. Morphological studies of the Additives

FE-SEM images of CCO, SCCO and IL-CCO were taken to find out their morphological features and are described in **Fig. 4.1**. The CCO nanoparticles of almost spherical shape and 12-15 nm size with slight agglomeration are visible in **Fig. 4.1a**. In **Fig. 4.1b**, capping by sodium dodecyl sulfate has reduced the size of NPs to 9-11nm. **Fig. 4.1c** and **4.1d** exhibit ionic liquid wrapped around NPs with the size of NPs reduced to 7-11 nm. The intense peaks in the EDX spectrum of IL-CCO, Figure 1e for carbon, nitrogen, oxygen, fluorine, sulfur, calcium and cerium manifest that the adsorbed film is made up of NPs and ionic liquid.

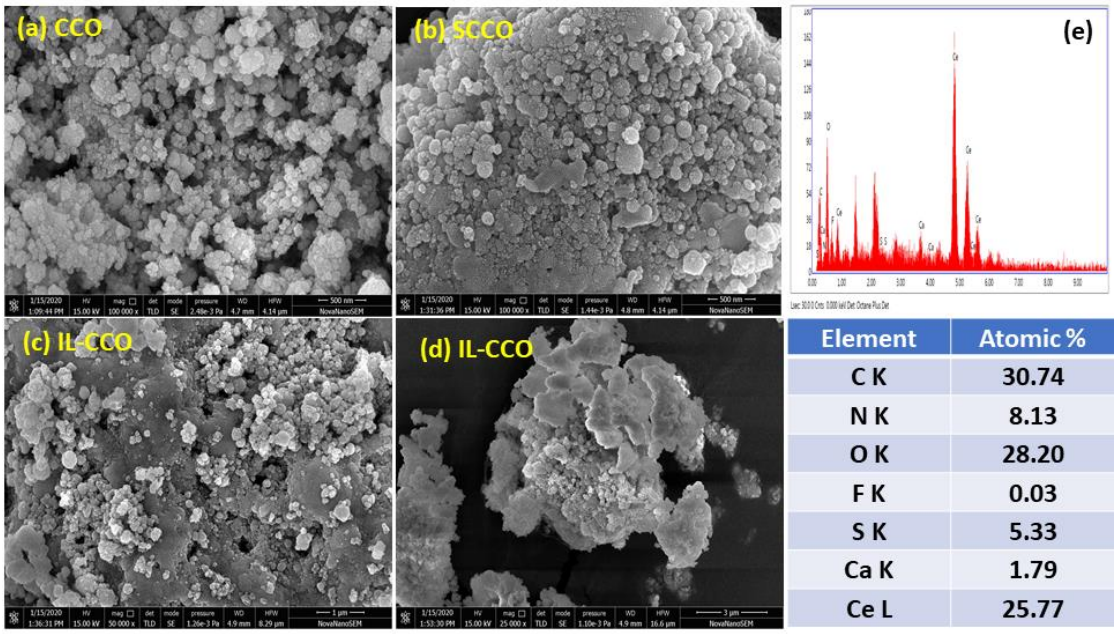

Element	Atomic %
C K	30.74
N K	8.13
O K	28.20
F K	0.03
S K	5.33
Ca K	1.79
Ce L	25.77

Fig. 4.1. FE-SEM images of (a) CCO (b) SCCO (c), (d) IL-CCO and (e) EDX spectra of IL-CCO

For a better perception of the morphology, the TEM /HR-TEM images of CCO and IL-CCO have also been taken and exhibited in **Fig. 4.2 (a, b)**. The spherical NPs with little agglomeration can be seen in **Fig. 4.2a**. The size of NPs appears to be in the range 7-15 nm, roughly similar to that calculated from FE-SEM studies. **Fig. 4.2b** shows again the NPs surrounded by the ionic liquid. The size of NPs was found as 5-10 nm (9-11nm from FE-SEM). The HR-TEM image of IL-CCO shows fringes, but being covered by the ionic liquid, the image looks like faded and lattice fringe distance could not be calculated.

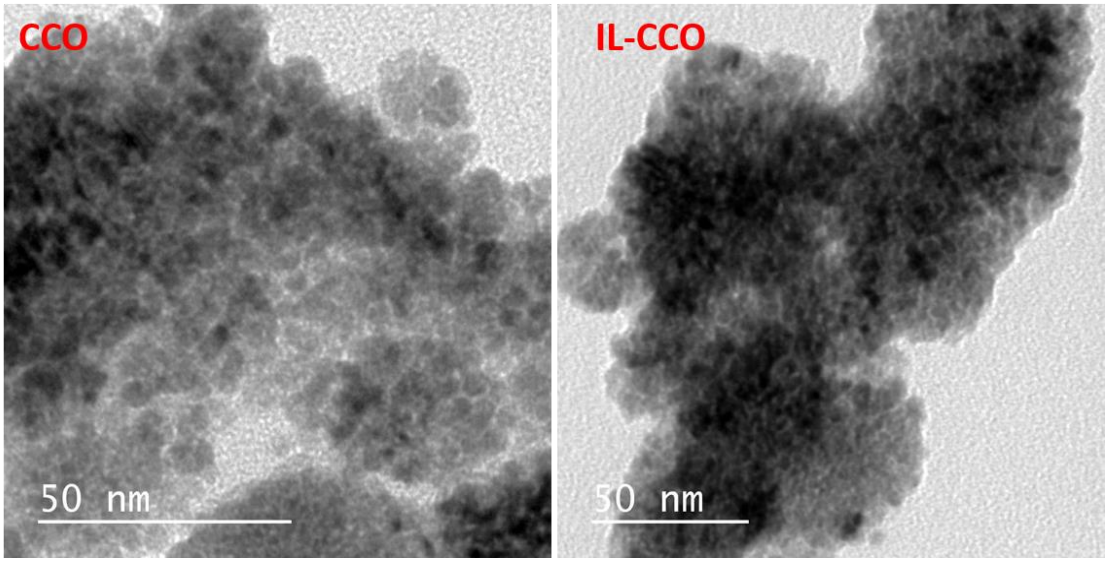

Fig. 4.2. TEM images of (a) CCO and (b) IL-CCO

The X-ray diffraction (XRD) patterns of CCO, SCCO and IL-CCO are displayed in Figure 3. The diffraction peaks appearing at 28.64°, 33.06°, 47.50°, 56.36°, 59.07°, 69.3°,7 6.68° and 78.87° corresponded to (111), (200), (220), (311), (222), (400), (331), (420) planes of ceria respectively. The observed diffraction peaks could be indexed for the cubic phase of ceria according to standard JCPDS file no.34-394 [Ramasamy et al. (2018)]. The absence of any additional peak due to calcium in the diffraction pattern of CCO, SCCO and IL-CCO indicates that calcium is doped in the cubic structure of ceria.

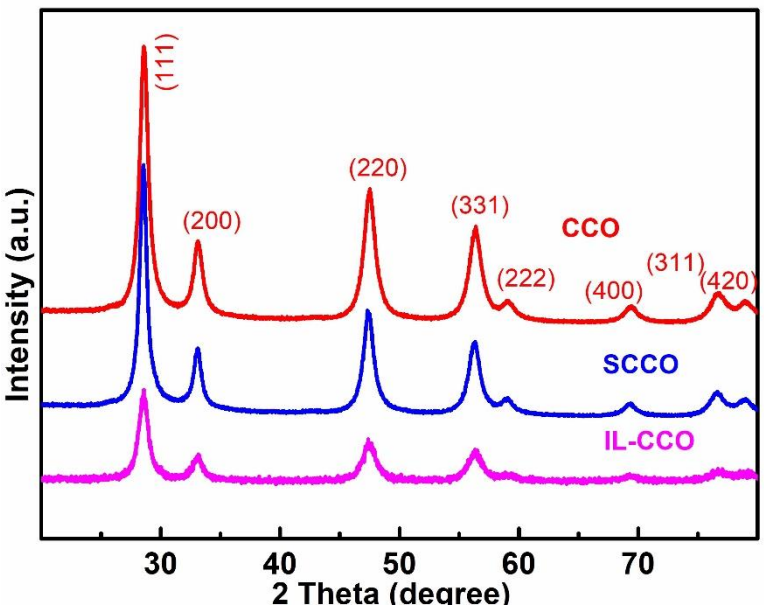

Fig. 4.3. XRD patterns of as-prepared CCO, SCCO and IL-CCO

Fig. 4.4 shows FTIR spectra of Ca doped ceria nanoparticles (CCO) and IL-CCO in the region 4000–400 cm^{-1}. The bands at 3404, 1553 and 1384 cm^{-1} in the spectrum of CCO are assigned to O-H stretching, scissor bending of C-O-H vibration and the characteristic band of CeO_2, respectively. These bands remain unaffected in IL-CCO. The bands due to stretching modes of Ca-O, CO_3^{2-} (due to atmospheric CO_2) at 1053, 840 cm^{-1} respectively, for Ce-O at 700 and 500 cm^{-1} in the spectrum of CCO are observed almost at similar positions in IL-CCO. Besides these bands of CCO, the spectrum of IL-CCO exhibits imidazolium ring vibrations (N(CH)NCH) at 3161 cm^{-1} and bands due to alkyl chain at 2848 and 2923 cm^{-1}. The IR bands, due to bis (trifluoromethyl sulfonyl) imide $Tf2N^-$ anion are observed in the range 1000-1400 cm^{-1} [Ramasamy et al. (2018)].

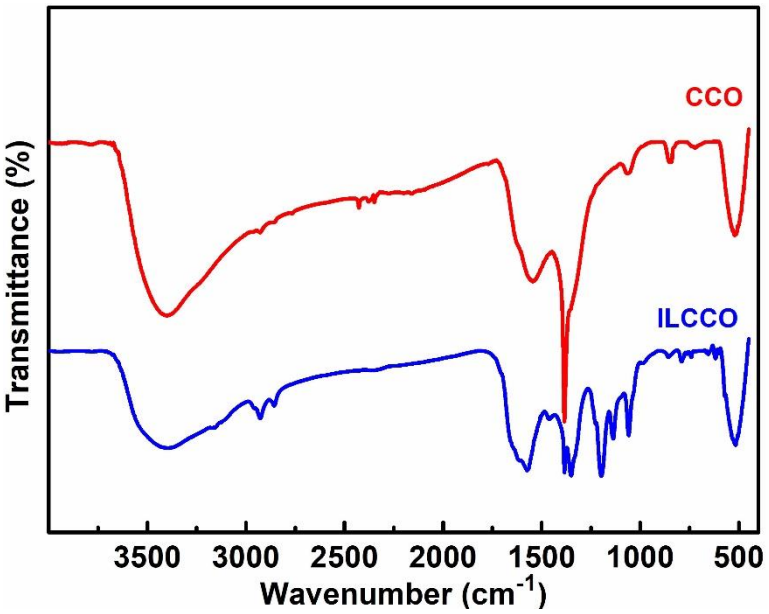

Fig. 4.4. FT-IR spectra of CCO and IL-CCO

4.2.2. Evaluation of tribological properties

4.2.2.1. Dispersion stability of nanofluids in a base oil

UV/visible spectroscopy was employed for determination of dispersion stability of the studied additives. The admixtures (0.2% w/v) were diluted ten times, and their absorbance values were recorded in the region 200-600 nm at six-hour intervals up to forty-eight hours. In the inset, the characteristics of absorbance values for dispersion of IL-CCO at 360 nm from zero to 48 h at six-hour intervals have been displayed. As expected, the absorbance drops with time within the test period. Figure 5a illustrates the relative absorbance of all the admixtures against settling time. The relative

absorbance decreases almost continuously with time, usually for all additives. However, the decrease is a little gradual in case of IL-CCO after 24 h. It is apparent from **Fig. 4.5a** that the extent of reduction of relative absorbance declines from CCO to IL-CCO through SCCO. All the additives have adequate stability as the relative absorbance decreases from 1.0 and reaches up to 0.543 in case of CCO, 0.561 for SCCO finally 0.623 for IL-CCO. **Fig.4.5b** presents direct photographs of base oil and its admixtures in the beginning and after 48 h divulging their stability.

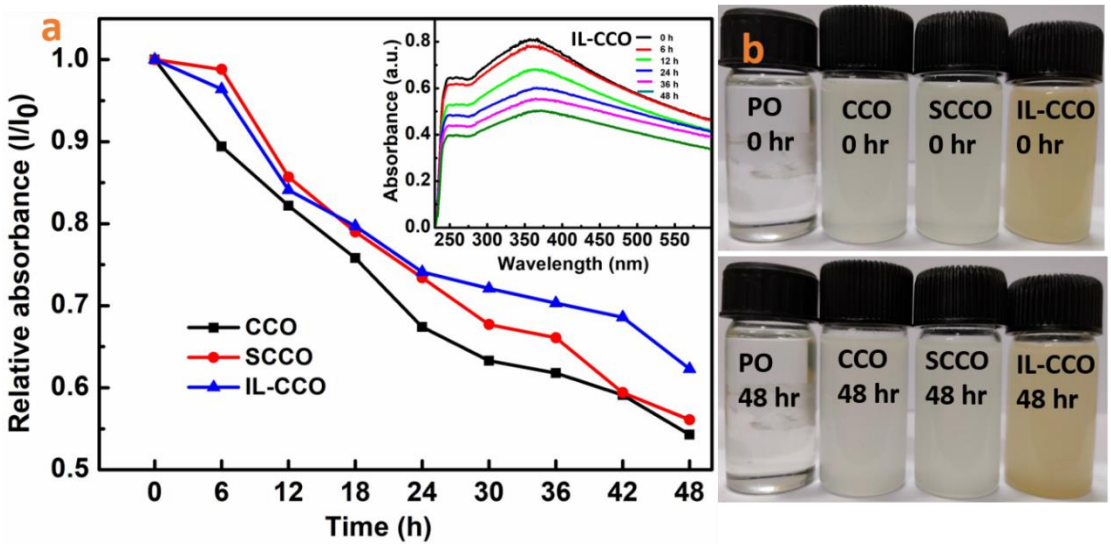

Fig. 4.5. (a) Dispersion stabilities of base oil containing CCO, SCCO and IL-CCO studied by UV-vis spectrophotometry. (b) Optical photographs of additives dispersed in base oil at different within 48 h

4.2.2.2. Additive optimization

The optimization of concentration was carried out by preparing blends of the additives, CCO, SCCO and IL-CCO having concentration as 0.00,0.10, 0.20, 0.30 and 0.40 %w/v in PO and the corresponding values of mean wear scar diameter (MWD) were noted under the test condition, 392 N applied load for 60 min. The accumulated data are

displayed in **Fig. 4.6**. Compared to the plain oil, a substantial decrease in MWD is observed for the blends at all the concentrations. At each concentration, the magnitude of the decrease is maximum for IL-CCO and least for CCO. The concentration of 0.2 %w/v is unique since the values of MWD are minimum for all the additives. However, there is a slight increase in MWD in every case at the next tested concentration, 0.3 %w/v. Afterwards, the MWD is stabilized or increase a little bit. Thus, 0.2 %w/v was finalized as the optimum concentration, and all the tests have been conducted at this concentration. It can also be concluded that the addition of ionic liquid has surmounted the antiwear activity of NPs alone or capped by sodium dodecyl sulfate.

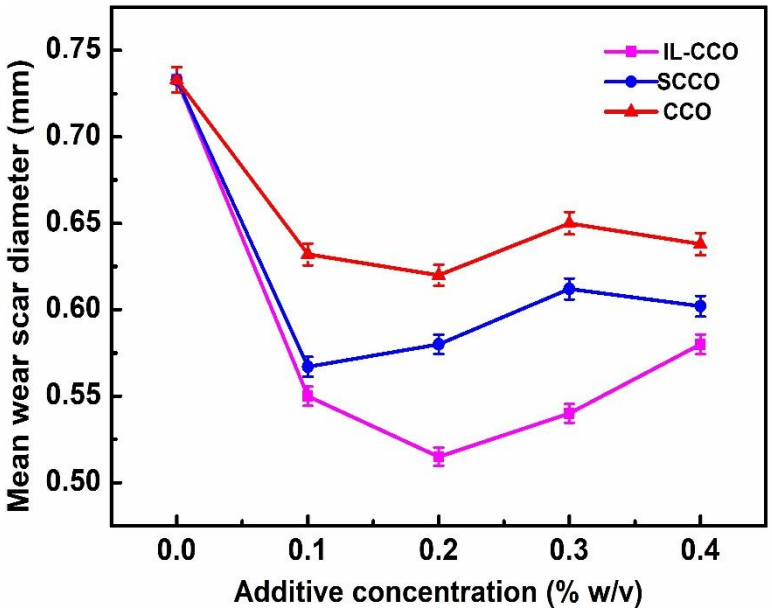

Fig. 4.6. Variation of mean wear scar diameter as a function of additive concentration (392 N, 60 min)

4.2.2.3. Diminution of friction and wear

The antiwear activity of base lube and its admixtures with the investigated additives having 0.2% w/v concentration was evaluated under ASTM D4172 conditions; 392 N load at 1200 rpm for 60 min. **Fig. 4.7** is a simultaneous presentation

of variation of mean wear scar diameter (MWD) and the average coeficient of friction (COF). The value of MWD in the presence of base lube, 0.733 mm undergoes diminution when CCO is blended with it (0.62). The reduction continues for the additive SCCO (0.58), and finally, with IL-CCO, it is minimum (0.515).

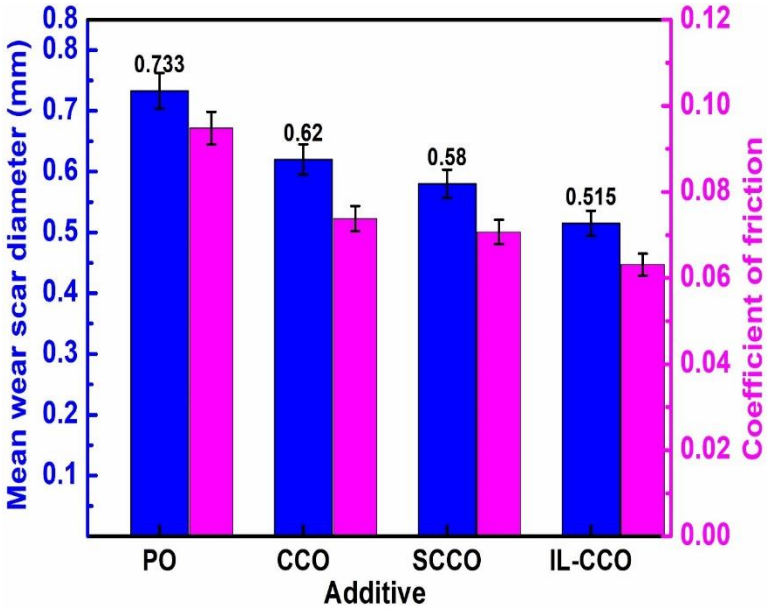

Fig. 4.7. Comparative analysis of wear scar diameter and coefficient of friction (COF) of different additives at an optimum concentration of 0.2% (w/v) in PO (392N, 60 min)

Likewise, the average coefficient of friction (COF) between the mating surfaces exhibits a similar pattern, i.e., highest for blank oil, decreases continuously from the blends of CCO, SCCO to IL-CCO. **Fig. 4.8** delineates the variation of COF with time. The COF is high in the initial phase because tribofilm formation is yet to start. With the formation of tribofilm, indeed, there is a lowering of COF until it becomes steady.

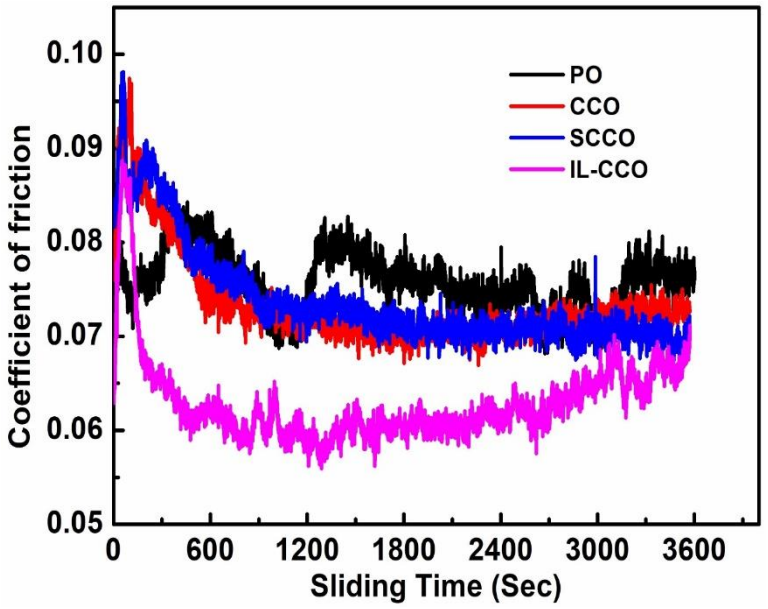

Fig. 4.8. Variation of the coefficient of friction with time (392 N, 1200 rpm, 3600 sec) for the studied additives in PO

4.2.2.4. Load-bearing capacity

The ASTM D-5183 test standards were applied to determine the load-bearing ability of plain oil alone and along with additives. After almost completion of the running-in period under the conditions, 392 N load, 600 rpm, 75°C temperature and 60 min, test was carried out by adding 98 N load at every 10 min interval till the seizure load is achieved. **Fig. 4.9** is a combined presentation of variation of frictional torque with time and load for base oil and its admixtures with additives.

The load-bearing capacity was found to be improved from base oil (980N) to the admixtures, CCO (2058N), SCCO (2254N) and IL-CCO (2352N). Obviously, in the case of IL-CCO, the tribofilm is long-lasting supporting the highest load.

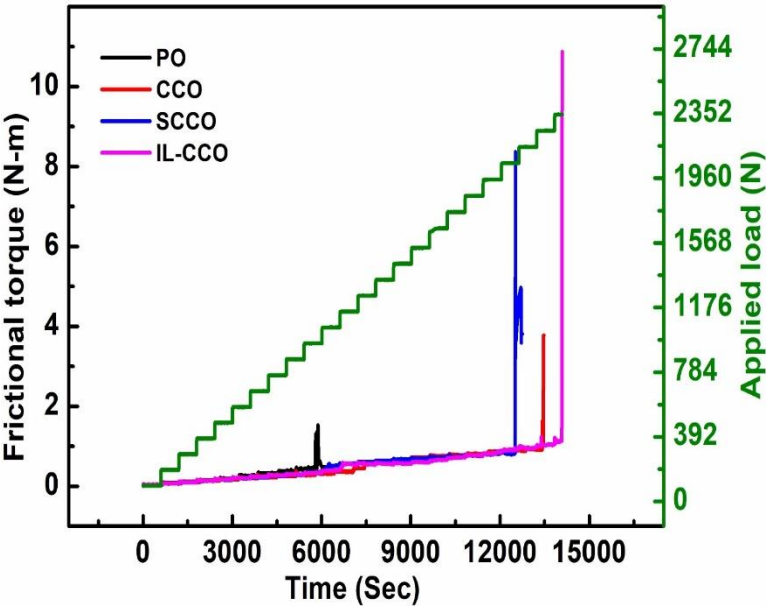

Fig. 4.9. Variation of frictional torque as a function of stepwise loading and time for PO in absence and presence of different nano additives: sliding speed, 600 rpm; temperature, 75^{o}C; concentration of additives, 0.2% w/v

4.2.2.5. Frictional power loss

Frictional power loss was determined using data from antiwear tests in the following equation

$$P = \mu N.r.\ \pi dn/60 \qquad 4.1$$

Where, P is the frictional power loss (N.m.s^{-1}); N is contact load on three balls, and r is the frictional radius, d is frictional diameter and n= 1200 rpm. Substituting all values in Eq. [1], the frictional power loss

$$P = 3.6 \times 2.07 \times \mu\ (MJ) \qquad 4.2$$

Table 4.1: Loss of frictional power measured of different additives at 0.2%w/v concentration

S.N.	Additives	Power consumption (MJ)	Reduction in Power consumption	% Reduction in Power consumption
1.	PO	0.706	----------	----------
2.	CCO	0.549	0.157	22.3
3.	SCCO	0.526	0.180	25.4
4.	IL-CCO	0.470	0.236	33.4

The frictional losses are inherently associated with longevity of machine components. Concerted efforts are being made to minimize frictional losses somehow and thus enhance the working efficiency of machine components. The frictional power losses are shown in Table1 in the presence of an optimum concentration of the different additives. The frictional power loss value in the presence of plain PO was observed as 0.706 MJ. Its blends with various additives cause a severe reduction in the frictional power loss. As apparent from the table, maximum reduction, 34% was achieved for the additive IL-CCO. It shows that ionic liquid modified CCO composite acts as excellent energy saviour [Rawat et al. (2019)].

4.2.3. Surface Characterization

4.2.3.1. Morphological studies of wear scar surface

The SEM images of the wear scar developed after ASTM D4172 test in the presence of oil with and without additives are shown in **Fig. 4.10**. The surface lubricated with plain oil exhibits furrowed structure. However, in the presence of additives, smoothness of

the surface has increased effectively. The relative smoothening of the surface follows the order of antiwear /antifriction activity of the additives. The inset in each figure depicts corresponding MWD. The attenuation of MWD from plain oil is compatible with the improvement of evenness of the surface. The EDX analysis of surface lubricated with CCO-IL affords the elemental makeup of the worn surface. Figure 10 divulges signals for the elements of CCO and IL-CCO; C, N, O, F, S, Ca, Fe and Ce indicating their vital role in the formation of tribofilm resulting in remarkable tribo performance.

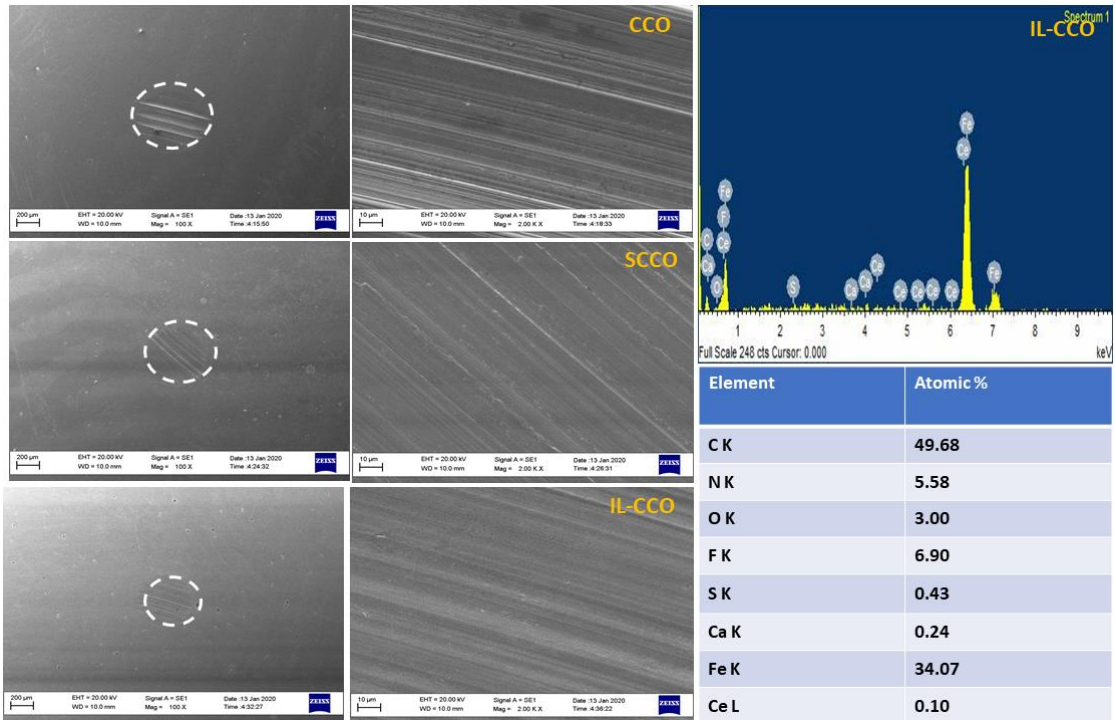

Element	Atomic %
C K	49.68
N K	5.58
O K	3.00
F K	6.90
S K	0.43
Ca K	0.24
Fe K	34.07
Ce L	0.10

Fig. 4.10. SEM micrographs (magnification 200 k X and 2.00 k X) of the worn steel surface lubricated with paraffin oil with different nano additives (0.2 % w/v) for 60 min test duration at 392 N applied load and EDX spectra of worn surface lubricated with IL-CCO

Morphological characteristics of the surface of the balls after the antiwear test (392 N load, 1h, 1200 rpm, 75 ^{o}C) performed in the presence of plain base oil and its blends

with the synthesized additives, were studied by AFM. **Fig. 4.11** describes *3D* images of the worn surfaces along with roughness data in the form of line roughness (Rq) and area roughness (Sq). The Rq and Sq values for the oil alone (Rq=295, Sq=370) experience massive degradation when mixed with various nano additives; CCO (Rq=214, Sq=258), SCCO (Rq=209, Sq=235) and IL-CCO (Rq=37, Sq=111). Thus, the roughness data obtained from AFM studies also endorse the tribological data.

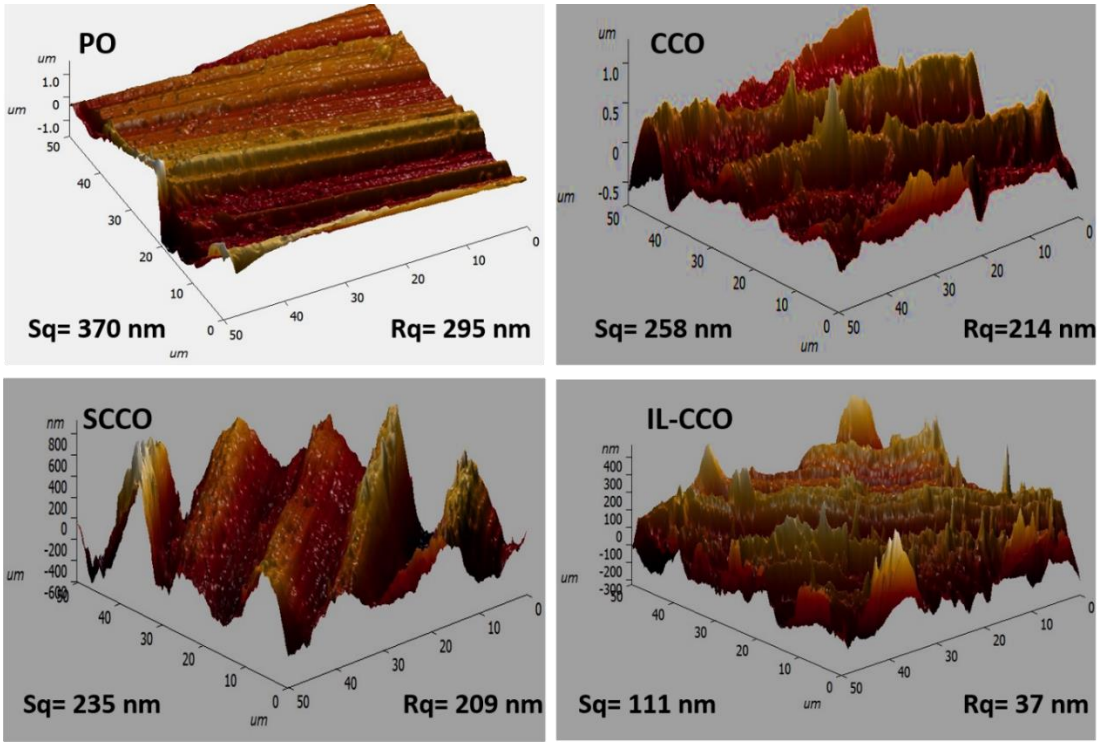

Fig. 4.11. *3D* AFM images of the worn steel surface lubricated with blank paraffin oil (PO) and blends of PO with 0.2 % w/v nano additives at 392 N applied load

4.3. Conclusions

Calcium doped ceria nanoparticles (CCO)prepared by sol-gel method were subjected to surface modification by sodium dodecyl sulfate and an ionic liquid,1-decyl-3-methyl imidazolium bis (trifluoromethylsulfonyl) imide to yield SCCO and IL-CCO,

respectively. The above syntheses were confirmed by FTIR and p-XRD techniques. Based on FE-SEM studies, the size of CCO nanoparticles decreased in SCCO and was minimum for IL-CCO. Indeed, effective wrapping of IL around NPs decreased the size. The significant increase in load carrying capacity, antiwear and antifriction efficiencies of IL-CCO in paraffin oil was obtained. Consequently, power consumption was reduced due to decreased frictional losses. The phenomenal advancement of tribological activity of IL-CCO could be attributed to the smallest size leading to swift tribo action. Further, the lubricating behaviour of ionic liquid has also played a significant role in enhancing the activity. The SEM and AFM studies of the wear track approved the findings from tribological data. EDX analysis of the wear scar surface lubricated with IL-CCO shows the presence of all its elements validating its strong adsorption on the surface resulting in high activity. All the nanoparticles CCO, SCCO or IL-CCO followed rolling, polishing and mending mechanisms for tribological activity.